Second-Generation UAM Community Noise Assessment Using the FAA Aviation Environmental Design Tool

Stephen A. Rizzi*
NASA Langley Research Center, Hampton, VA 23681, USA

Menachem Rafaelof†
National Institute of Aerospace, Hampton, VA 23666, USA

Vehicles serving the urban air mobility (UAM) market are anticipated to operate in communities close to the public at large. The approved model for assessing environmental impact of air traffic actions in the United States, the Federal Aviation Administration's Aviation Environmental Design Tool (AEDT), does not support analysis of such operations due to a combined lack of a UAM aircraft performance model and aircraft noise data. This paper discusses second-generation developments to assess the acoustic impact of UAM fleet operations on the community using AEDT and demonstrates its use for representative UAM operations. In particular, methods were developed to add broadband self noise into computed noise-power-distance data, and vertiport-centric operations were evaluated for two concept vehicles.

I. Introduction

IN the US, the FAA Aviation Environmental Design Tool (AEDT)[1] is the required tool to assess aircraft noise and other environmental impacts due to federal actions at a civilian airport or vertiport, or in US airspace for commercial flight operations. AEDT and prediction tools with the same or similar modeling technologies are used in other countries as well.[2] For fixed-wing aircraft, AEDT calculates various noise metrics using Noise-Power-Distance (NPD) data specific to each aircraft. In its customary mode of operation, the AEDT performance model determines the engine power required to execute the specified flight operation. The noise data are interpolated for power and distance, along with various adjustments, to estimate the sound exposure at a set of receptors on the ground. For rotary-wing aircraft (helicopters), AEDT calculates sound exposure using Noise-Operating Condition-Distance (still termed NPD) data specific to each vehicle, with the operating condition, e.g., hover, directly specified through a procedure step, and not by engine power.

There are some obstacles to using AEDT for assessment of community noise due to urban air mobility (UAM) vehicle operations. The first is that there are no available NPD data for UAM vehicles, whether the vehicles are modeled as fixed-wing or rotary-wing type vehicles within AEDT. Secondly, when modeling a UAM vehicle as a fixed-wing type, there are no performance data available to determine required engine power. When modeling a UAM vehicle as a rotary-wing type, the number of defined operating conditions within AEDT are limited to a few that are appropriate for typical helicopter operations, but may be insufficient for describing UAM operations.

A recent white paper[3] established a set of high-level goals to address key issues associated with UAM noise. One of these goals is to examine UAM fleet noise impacts through prediction and measurement, along with a recommendation that "*Research be conducted to more fully explore limitations in methods for assessing community noise impact of UAM vehicles in their operational environments, and to generate a software development plan that addresses the limitations of current models over time*." To that end, this paper describes new developments for assessing UAM community noise using the standard distribution of AEDT, i.e., without modification. The first-generation (Gen 1) NPD data[4] for two reference UAM vehicles were based solely on periodic loading and thickness noise. In the second-generation (Gen 2) analyses, the data are augmented to include broadband self noise. Additionally, the modeling methodology used in the Gen 1 noise assessments,[4] i.e., using fixed-point flight profiles in the fixed-wing mode, was targeted at particular vertiport(s) within a wide area network of vertiports in Gen 2. In this paper, the Gen 2 data and modeling methodology are used to assess UAM community noise at a candidate vertiport in the Dallas-Ft. Worth area.

---

* Senior Researcher for Aeroacoustics, Aeroacoustics Branch, AIAA Fellow
† Senior Research Engineer

II. Concept Vehicles, Scenario, and Operating States

A. Vehicle Description

Two reference vehicles developed under the NASA Revolutionary Vertical Lift Technology (RVLT) Project were included in this investigation, namely, the quadrotor and "lift plus cruise" (L+C) vehicles, see Figure 1. Both vehicles were sized for a 1200 lb. payload (up to six passengers) executing a representative mission profile.[5] The quadrotor was an all-electric variant, with three-bladed rotors each with a radius (R) of 13.1 ft, gross weight of 6469 lb., and maximum airspeed V_{max} of 109 knots true airspeed (KTAS). The L+C was a turboelectic variant, with eight two-bladed lifting rotors each with R=5 ft., a three-bladed pusher propeller with R=4.5 ft., gross weight of 5903 lb., and V_{max} of 123 KTAS. Additional details on these configurations can be found in Silva et al.[6]

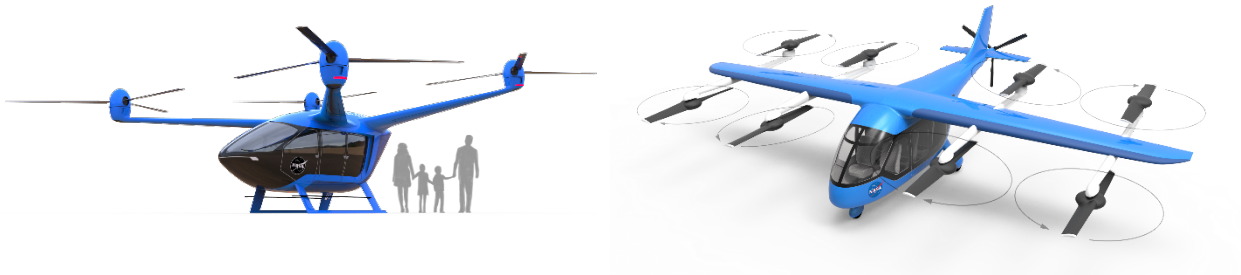

Figure 1: NASA RVLT reference vehicle configurations considered in this study: quadrotor (left) and lift plus cruise (right).

B. Scenario Data

The route structure used in this study is significantly more complex than the sixteen routes in the Dallas-Ft. Worth area that were considered in the first-generation study.[4] Input scenarios were derived from the Virginia Tech common scenarios,[7] and adjusted to remove, relocate, or combine vertiports located inside UAM usable airspace. UAM routings were derived using a route network search algorithm to include UAM unusable airspace and previously designed UAM routes.[8] Trajectory data were generated using the UAM Mission Planner[9] with all constraints enabled (e.g., vertiport scheduling and fleet management), but with predeparture conflict detection and resolution (CD&R) disabled. A 60 s interoperation (slot) time was used between operations on the same vertipad at a vertiport. The resulting UAM flights include those carrying passengers and those used for fleet management (repositioning and clearing). The route structure, shown in Figure 2, consisted of 46 vertiport sites and approximately 10,000 daily takeoff and landing operations. Additionally, the scenarios include 4 storage facilities that facilitated fleet management operations. It should be noted that scenarios run with and without predeparture CD&R would result in a different set of flights and trajectories, and that noise assessments represented in this work are specific to the scenario and vehicles described herein.

The Mission Planner output of each simulated route consisted of the 4D trajectory (time, latitude, longitude, and altitude), heading, ground speed, and rate of climb, at a 1 Hz sampling rate. Simulated flights for each vehicle had a nominal cruise speed of roughly 85% of V_{max}. The trajectories for the quadrotor and L+C vehicles differed slightly from one another due to differences in their flight dynamics models. In the subsequent AEDT analyses, the trajectories used were those associated with the respective vehicle. Vertiport DF1, having 3 vertipads and located in downtown Dallas, was selected as the focus of this study because of its high number of daily operations (totaling 1119), and its high degree of connectivity with the other vertiports. Vertiport DF1 shares operations with 40 of the remaining 45 vertiports and 3 of 4 storage facilities. Figure 3 shows arrival operations at vertiport DF1 that originate from 38 vertiports and 3 storage facilities. Figure 4 shows departure operations from vertiport DF1 with destinations at 38 vertiports and 1 storage facility. The set of vertiports and storage facilities in Figure 3 differ from those in Figure 4 because of the existence of operations besides those to and from vertiport DF1, as depicted in Figure 2.

The hourly distribution of arrivals and departures to and from vertiport DF1 is shown in Figure 5. Here, the flights are binned by the hour of their departure from the originating vertiport. The bimodal distribution reflects increased activity during the morning and afternoon rush hours, and shows much fewer operations during the nighttime hours between 10 PM (hour 22) and 7 AM (hour 7). The uptick in early morning operations between 5-7 AM occurs during this period and these operations are therefore subject to the nighttime penalty of 10 dB when computing the day-night average sound level (Ldn). Vertiport DF1 has the expected imbalance of passenger demand with many commuter trips coming into the city in the morning, and many commuter trips leaving the city in the afternoon. However, due to the limited surface capacity of the vertiport, the number of arrivals and departures

appear to be about the same both in the morning and in the afternoon. In the morning, the majority of arrivals are flights carrying passengers into the city while the majority of departures are clearing flights making room for the incoming demand (once the vertiport is full, each arrival needs to be balanced by a departure). Similarly, in the afternoon, the majority of departures from the city are passenger carrying flights while the arrivals are repositioning flights that need to come into vertiport DF1 to carry those passengers out.

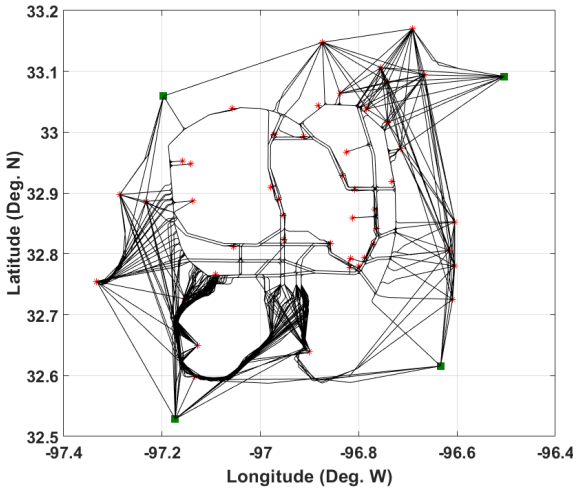

Figure 2: Entire route structure (—), vertiports (*), and storage facilities (■) that serves as the basis of the Gen 2 study.

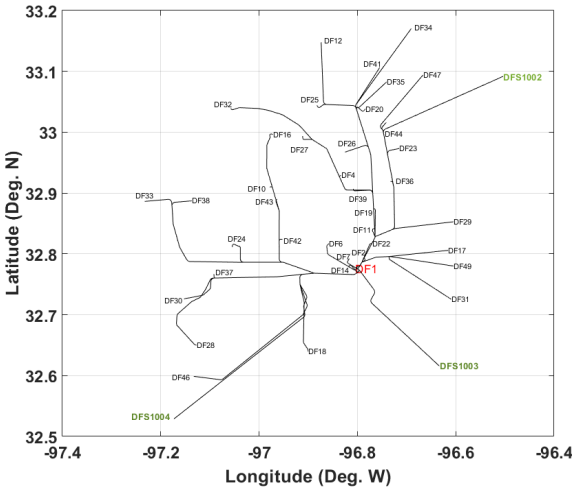

Figure 3: Subset of routes arriving at vertiport DF1.

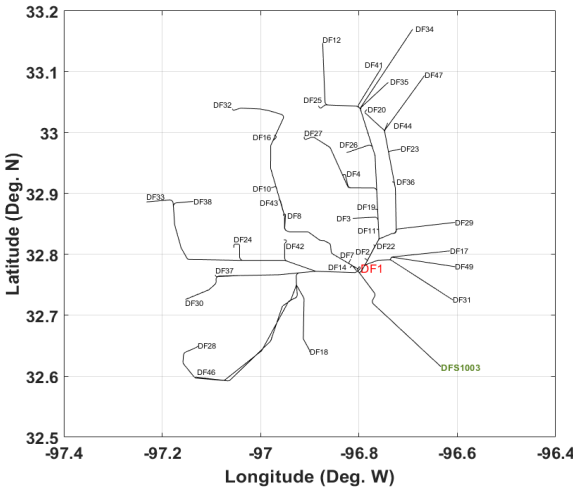

Figure 4: Subset of routes departing from vertiport DF1.

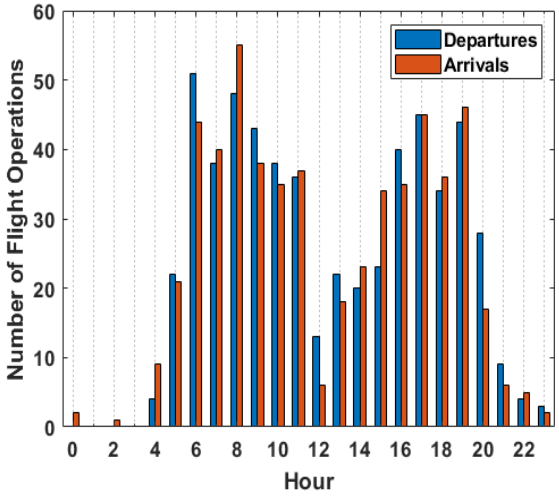

Figure 5: Hourly distribution of arrival and departure operations at vertiport DF1.

C. Determination of Operating States

As in the Gen 1 analyses, the aircraft operating states are defined by pairs of airspeed (knots) and climb angle (deg.). The new routes were not reanalyzed to determine a different set of operating states particular to this study. Instead, the operating states identified in the Gen 1 analyses were used for Gen 2. These were comprised of 42 and 44 unique operating states for the quadrotor and L+C vehicles, respectively, distributed in 10 knot increments of airspeed (from 0 to 0.85V_{max}), and in 5° increments of climb angle (from -90° in descent, to 90° in ascent). Since the source noise prediction process can be computationally intensive, only those operating states that had at least 10 occurrences in the Gen 1 4D trajectory data were evaluated. The set of Gen 1 operating states were compared with operating state data derived from the Gen 2 4D trajectory data and were found to adequately cover the range of conditions, see Figure 6. Note that the zero airspeed data are applied to all climb angles with airspeeds less than 5 knots.

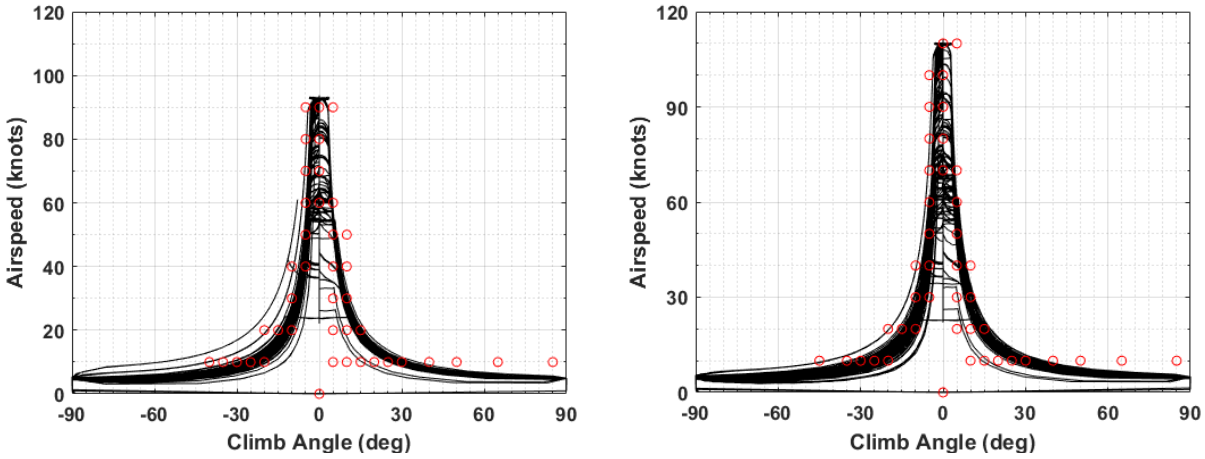

Figure 6: Operating states for the quadrotor (left) and L+C (right) vehicles. Black lines represent Gen 2 operating states derived from the 1 Hz trajectory data and red circles represent states identified in the Gen 1 study.

III. Noise-Power-Distance Data Generation

As previously mentioned, one of the impediments to using AEDT for assessment of community noise from UAM vehicle operations is the lack of noise-power-distance (alternatively noise-operational mode-distance for helicopters) or NPD data for UAM vehicles in the Aircraft Noise and Performance (ANP) database.[10] This section reviews the process for generating fixed-wing NPD data through analysis, including determining the trimmed conditions for each vehicle, performing an acoustic analysis to generate the source noise definition, and generating noise metrics at a ground receiver at a set of prescribed distances. A summary of each analysis step follows. The overall process is depicted in Figure 7, in which the script "pyaaron" executes all steps for each operating state.

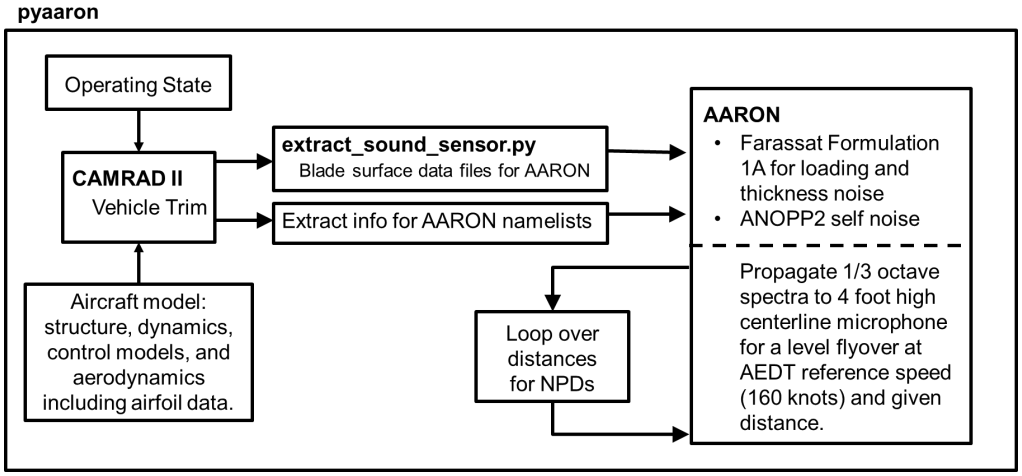

Figure 7: NASA process for generating Gen 2 fixed-wing NPD data.

A. Vehicle Trim

For a given vehicle configuration (quadrotor and L+C) and prescribed operating state, the vehicle is "trimmed" in an iterative fashion using a comprehensive analysis code. In the trimmed condition, the control surface configuration of the vehicle corresponds to the desired operating state (airspeed and climb angle). For this work, the Comprehensive Analytical Model of Rotorcraft Aerodynamics and Dynamics (CAMRAD II)[11] was used to trim the vehicles. Vehicle trim was performed in the same manner as that used in the Gen 1 assessment.[4] In addition to the blade loadings and motion used to compute periodic loading and thickness noise, CAMRAD II analyses were augmented to provide the angle of attack and the three components of induced velocity (due to wakes) as a function of rotor radius and azimuth. These additional data serve as partial input to the recently developed broadband self noise module in the NASA 2nd generation Aircraft NOise Prediction Program (ANOPP2).[12]

B. Source Noise Definition

Source noise data are generated using the ANOPP2 Aeroacoustic ROtor Noise (AARON) tool. The Gen 1 noise database[4] consisted of only periodic loading and thickness noise, computed using Farassat's Formulation 1A.[13] In this work, the source noise data are augmented with broadband self noise, following the formulation by Brooks et al,[14] as implemented in the ANOPP2 Self Noise Internal Functional Module (ASNIFM). Additional input data for the self noise analyses, apart from the CAMRAD II output, include the zero-lift angle of attack as a function of rotor radius and hover tip Mach number, and the trailing edge (TE) thickness and wedge angle as a function of rotor radius. Vehicle sizing using the NASA Design and Analysis of Rotorcraft (NDARC) code[15] specified the lifting rotor and cruise propeller blades to use a Sikorsky SSC-A09 rotorcraft airfoil table for the inboard section ($0 \le r/R \le 0.85$), a Boeing-Vertol VR-12 rotorcraft airfoil table for the outboard section ($0.95 \le r/R \le 1$), with an interpolation between those airfoil tables for intermediate stations ($0.85 \le r/R \le 0.95$). The zero-lift angle, shown in Figure 8, was calculated under a hover condition as a function of Mach number at each radial station. The sensitivity of the self noise calculation to the zero-lift angle has not been thoroughly investigated, so no effort was undertaken as part of this study to incorporate an azimuthal variation that would accompany any of the forward flight conditions. The TE thicknesses and wedge angles were not specified as part of the NDARC or CAMRAD II analyses. A constant TE thickness (scaled by rotor radius) and a constant TE wedge angle were specified based on representative data from the HART II rotor.[16] Since the self noise calculation is known to be sensitive to these TE parameters, the resulting self noise data are not considered to be generally applicable to other airfoil geometries.

The three noise components, periodic loading and thickness noise and broadband self noise, constitute the so-called Gen 2 NPD database. The particular database used in this work (Gen 2.2.2) includes the wake modeling improvements contained in the Gen 1.2 database.[4]

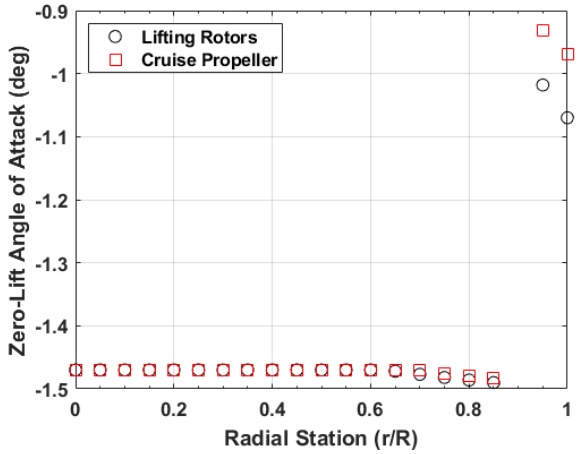

Figure 8: Zero-lift angle of attack used in the calculation of the broadband self noise component.

Table 1: Additional parameters used in the calculation of the broadband self noise component.

Rotor	TE thickness (mm)	TE wedge angle (deg.)
Quad Lifting Rotor	1.8	18
L+C Lifting Rotor	0.69	18
L+C Cruise Propeller	0.62	18

C. Noise Metrics

The process for generating noise metrics used in AEDT, including the maximum A-weighted sound pressure level L_{Amx}, the A-weighted sound exposure level L_{AE}, the maximum tone-corrected perceived noise level L_{PNTSmx}, and the effective tone-corrected perceived noise level L_{EPN}, follows that of the earlier work utilizing the fixed-wing aircraft type.[4] To recap, for fixed-wing aircraft, the above source noise definitions are "flown," through simulation, at the 160 knot AEDT reference speed and at the AEDT distances (the "Distance" in NPD) of 200, 400, 630, 1k, 2k, 4k, 6.3k, 10k, 16k, and 25k ft. above an observer under the flight path. A comparison of L_{AE} data is shown in Figure 9 for the quadrotor with (Gen 2) and without (Gen 1) broadband self noise. The addition of the broadband self noise component significantly increases the noise associated with vertiport departure operations (low speed with high climb angles) by about 30 dB and in the climb phase by about 10 dB. The increase in L_{AE} is not as great for the L+C (up to about 3 dB across all operating states), as shown in Figure 10. Full transition to wing-borne lift for the L+C vehicle is seen in the sudden drop in L_{AE} at airspeeds $\ge$ 70 knots.

It is helpful to examine differences in the Gen 2 data more directly for subsequent comparisons of community noise impact from the quadrotor vehicle relative to the L+C vehicle. From Figure 6, it is clear that the set of operating states (the particular pairs of airspeed and climb angle) for the quadrotor vehicle is not identical to that of the L+C vehicle. Many states, however, are common and differences between the Gen 2 data from Figure 9 and Figure 10 are shown in Figure 11. A positive difference indicates a greater level for the quadrotor vehicle, and a negative difference indicates a greater level for the L+C vehicle. Here it is seen that, for cruise conditions, the

quadrotor vehicle has higher levels than the L+C vehicle, as it does not benefit from lift generated by a wing. In contrast, the L+C vehicle has higher levels on takeoff and climb (departure), and, to a lesser extent, for higher speed descent conditions (arrivals) compared to the quadrotor vehicle.

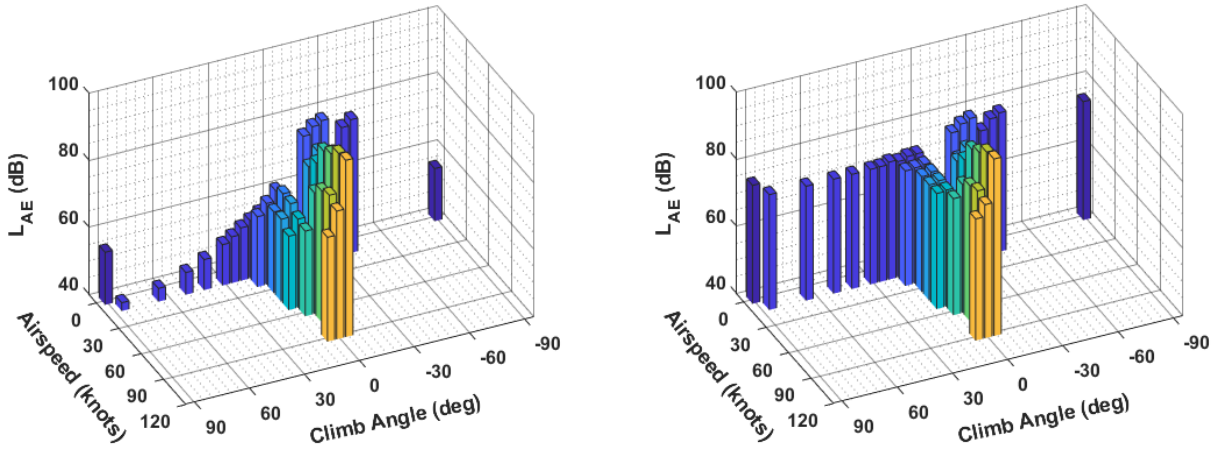

Figure 9: L_{AE} data for the quadrotor without (left) and with (right) broadband self noise at a distance of 200 ft.

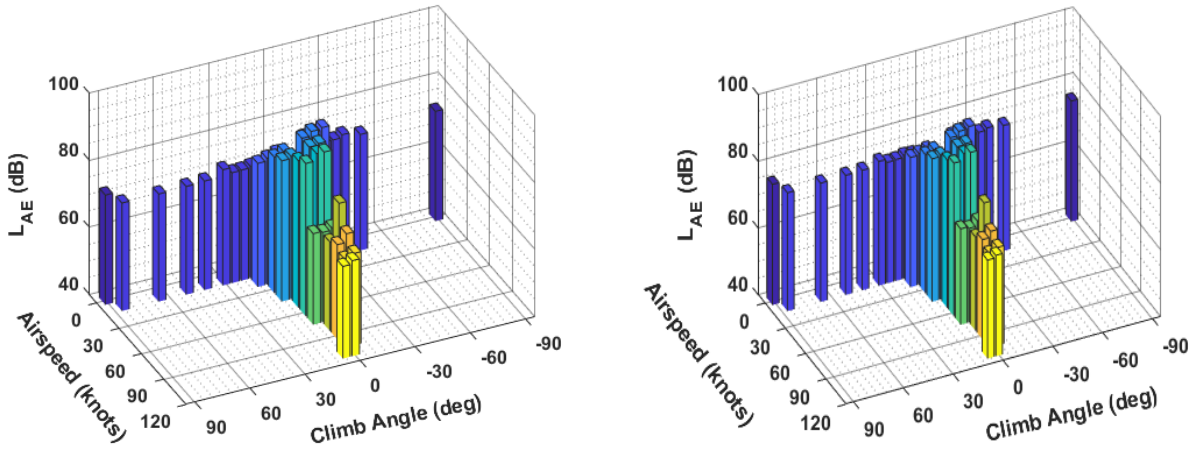

Figure 10: L_{AE} data for the Lift+Cruise without (left) and with (right) broadband self noise at a distance of 200 ft.

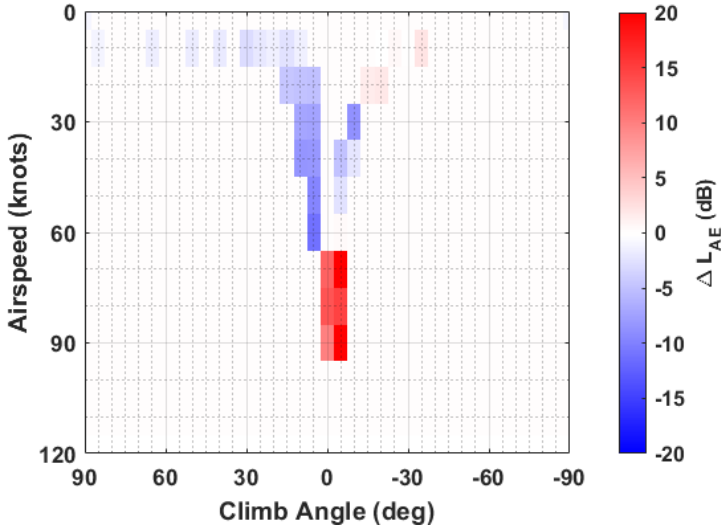

Figure 11: Difference in Gen 2 L_{AE} data (quadrotor minus L+C) at a distance of 200 ft.

IV. AEDT Modeling Approach

The modeling approach closely follows that used in the Gen 1 study,[4] namely use of fixed-point flight profiles in association with the fixed-wing aircraft type. The modeling has been constructed to assess noise due to arrivals at vertiport DF1, departures from vertiport DF1, or arrivals to and departures from vertiport DF1 combined. Recall that AEDT supports five types of flight operations for fixed-wing aircraft including approach, departure, overflight, circuit flight, and touch-and-go. Operation types cannot be combined into a single point-to-point operation; circuit flight and touch-and-go types are at the same airport, overflights start and end in the airspace, and approach and departure account for only one of two points (destination or origin). As in the Gen 1 study, departure type flight operations were used exclusively, with track points originating at one vertiport and ending at another. In other words, each flight operation begins as a departure from one vertiport and simply ends at the location of another vertiport. Subsequently, departures from vertiport DF1 use the departure type with the track originating at DF1 and ending at the destination vertiport or storage facility. Arrivals to vertiport DF1 also use the departure type, but with the track originating at a vertiport or storage facility other than vertiport DF1 and ending at destination vertiport DF1.

Track points define the 2D (x-y) routes and are constructed in a manner that accounts for heading changes. Arrival and departure tracks are unique, e.g., the track departing vertiport DF1 and arriving at vertiport DF30 is not simply a reversed version of the track departing vertiport DF30 and arriving at vertiport DF1. Consequently, there are a total of 160 sets of track points in the study. Specifically, for each vehicle, there are 39 unique tracks arriving at vertiport DF1 and 41 unique tracks departing from vertiport DF1. The track and vertiport data were written to AEDT standard input file (ASIF)[17] 'study' files as the means of inserting these data for analysis.

Each route was analyzed in an automated fashion. A sequential set of profile data for each route and vehicle, consisting of the segment number, cumulative distance along the ground track, altitude (ft. above field elevation), average airspeed, operational state identifier, and operation mode (always departure) was written along with the NPD data to an 'ANP' ASIF file for insertion into AEDT. Unlike the Gen 1 study,[4] the present study incorporates the variation in distance to each receptor due to the local terrain. There are as many sets of profile points as there are sets of track points.

A total of 1119 daily flights in and out of vertiport DF1 were specified in this study. A detailed breakdown of daytime and nighttime flights for arrivals to, and departures from, vertiport DF1 is provided in Table 2. Daytime and nighttime flights arriving at vertiport DF1 number 470 and 84, respectively, while those departing vertiport DF1 number 481 and 84, respectively. The difference in the number of departing and arriving flights is a result of the scenarios starting with a non-zero number of vehicles at the vertiports. Consequently, this demand model requires specification of 248 nonzero flight operations within AEDT (124 for each vehicle). There are 68 flight operations (41 daytime and 27 nighttime) arriving at DF1, and 56 flight operations (39 daytime and 17 nighttime) departing from DF1, constituting an overall proportion of 85% of daytime operations and 15% of nighttime operations.

V. Results

Analyses were conducted for daily operations consisting of three fleet mixes: 100% quadrotor vehicles, 100% L+C vehicles, and a mix of 50% quadrotor and 50% L+C vehicles. For the 100% fleet mixes, community noise assessments were conducted for arrivals at vertiport DF1 only, departures from vertiport DF1 only, and combined arrivals to and departures from vertiport DF1. For the 50/50 fleet mix, community noise assessments were conducted only for combined arrivals to and departures from vertiport DF1. For each assessment, Ldn was evaluated over two different receptor grids: a 500 x 500 grid spanning a 1674 sq. nm area (fully covering all vertiports and storage facilities) with a uniform grid spacing of 498 ft., and a 250 x 250 grid spanning a 24.8 sq. nm mile area (in the vicinity of vertiport DF1) with a uniform grid spacing of 121.5 ft.

Because of occurrences of an odd number of daytime and nighttime flights, it was not possible to construct the analysis of the 50/50 fleet mix by attributing half the number of flights to the quadrotor vehicle and half the number of flights to the L+C vehicle, since AEDT can only handle an integer number of flights. Therefore, the 50/50 fleet mix analyses were conducted by reducing Ldn values at each receptor by 3 dB for each vehicle at 100%, then adding according to

$$\mathrm{Ldn}_{50/50}(\mathrm{dB}) = 10\log_{10}\left[10^{\frac{\left(\mathrm{Ldn}_{\mathrm{quad}}-3\right)}{10}} + 10^{\frac{\left(\mathrm{Ldn}_{\mathrm{L+C}}-3\right)}{10}}\right]. \quad (1)$$

This is equivalent to halving the number of operations of each vehicle type.

Table 2: Breakdown of daily daytime and nighttime flights to and from vertiport DF1.

Originating Site (Arrivals to DF1)	Number of Daytime Flights	Number of Nighttime Flights	Destination Site (Departures from DF1)	Number of Daytime Flights	Number of Nighttime Flights
DF10	4	1	DF10	5	0
DF11	12	1	DF11	3	7
DF12	1	0	DF12	1	0
DF14	11	0	DF14	9	0
DF16	7	4	DF16	10	1
DF17	24	8	DF17	34	13
DF18	72	9	DF18	62	17
DF19	5	0	DF19	1	0
DF2	14	1	DF2	13	1
DF20	1	3	DF20	5	0
DF22	10	0	DF22	9	2
DF23	13	1	DF23	16	0
DF24	3	2	DF24	6	0
DF25	6	1	DF25	6	0
DF26	7	1	DF26	6	1
DF27	7	1	DF27	10	0
DF28	6	1	DF28	8	0
DF29	21	9	DF29	39	2
DF30	2	0	DF3	3	1
DF31	45	4	DF30	4	1
DF32	3	1	DF31	28	0
DF33	3	1	DF32	3	0
DF34	3	2	DF33	4	0
DF35	3	0	DF34	4	0
DF36	45	11	DF35	6	0
DF37	2	3	DF36	54	15
DF38	5	0	DF37	11	0
DF39	1	0	DF38	4	1
DF4	19	6	DF4	17	3
DF41	6	0	DF41	7	0
DF42	5	1	DF42	3	1
DF43	7	4	DF43	11	1
DF44	4	1	DF44	9	0
DF46	3	2	DF46	5	0
DF47	3	1	DF47	5	0
DF49	38	4	DF49	21	7
DF6	3	0	DF7	4	0
DF7	5	0	DF8	2	0
DFS1002	8	0	DFS1003	33	10
DFS1003	30	0	—	—	—
DFS1004	3	0	—	—	—

A. Full Operations Area Analyses

Noise exposure levels shown in Figure 12 – Figure 14 provide a bird's eye view of the full operations area. Noise exposure due to 100% quadrotor operations (Figure 12) relative to 100% L+C operations (Figure 13) is consistent with relative L_{AE} levels in Figure 11, with higher en route (between vertiports) exposure due to quadrotor operations relative to L+C operations. In both cases, the highest levels are found in the vicinity of the vertiports, with the greatest exposure at vertiport DF1 where all flights converge. As expected, noise exposure due to the 50/50 quadrotor/L+C operations mix lies in between the 100% quadrotor and 100% L+C cases, see Figure 14. Contour areas shown in Figure 15 indicate that the quadrotor exposure area is higher than the L+C exposure area at all but the highest Ldn level of 70 dB. Note that the contour areas in this and subsequent plots represent the entire area within a given contour level, e.g., the 65 dB contour level contains all receptors with exposures of 65 dB and greater.

Additional insight can be gained by evaluating the noise exposures due to arrivals only and due to departures only (see Figure 16 and Figure 17). Here, the larger contour area for the L+C vehicle at 70 dB is shown to be due to departure operations. This observation is consistent with Figure 11 in which it is shown that the L+C vehicle has higher departure noise than the quadrotor vehicle.

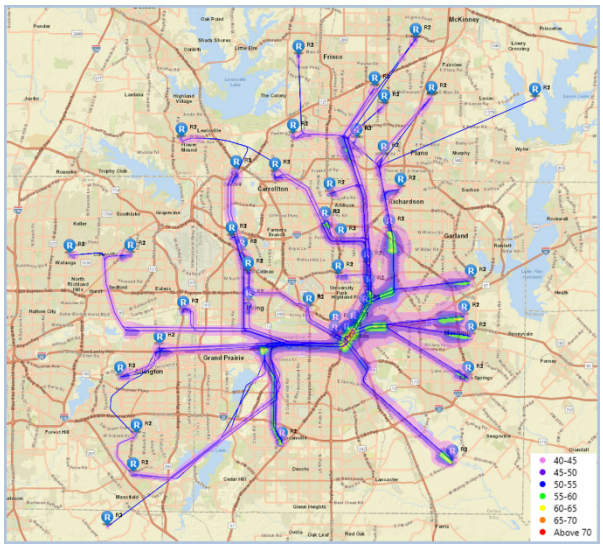

Figure 12: Noise exposure levels, Ldn (dB), for 100% quadrotor (arrival and departure operations).

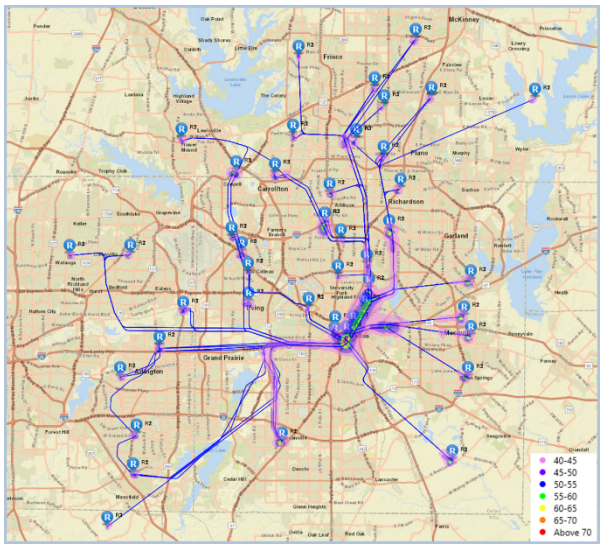

Figure 13: Noise exposure levels, Ldn (dB), for 100% L+C (arrival and departure operations).

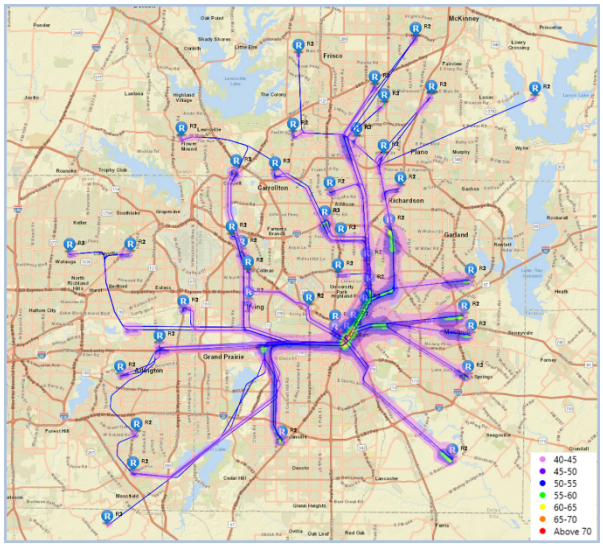

Figure 14: Noise exposure levels, Ldn (dB), for 50/50 vehicle mix (arrival and departure operations).

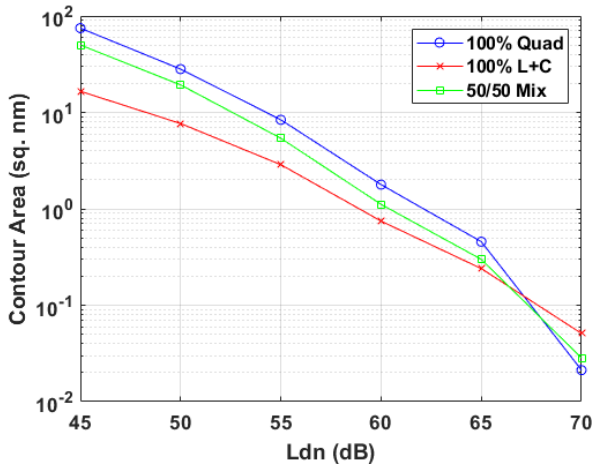

Figure 15: Ldn contour areas corresponding to Figure 12 – Figure 14.

B. Vertiport Area Analyses

The higher density receptor grid in the vicinity of vertiport DF1 is used to more closely examine the area with the highest noise exposure. Such a level of detail would be necessary to reduce noise exposure through modification of takeoff and landing operations. Note that this grid area also encompasses vertiports DF2, DF22, DF7 and DF14, see Figure 3 and Figure 4. The more detailed exposure maps shown in Figure 18 – Figure 20 are consistent with the full area view in the sense that the areas of lower contour levels for 100% L+C vehicle operations are significantly reduced from those associated with 100% quadrotor vehicle operations. The exposure areas for the 50/50 mix again fall in between those of the quadrotor only and L+C only cases. This is most clearly seen in Figure 21. Even on this

scale, the exposure areas are deceiving. For example, the 65-70 dB exposure area in Figure 18 extends for about 2 mi in the long direction and about 0.3 mi across (an area of roughly 60 city blocks @ 0.01 sq. mi.). The highest exposure level (above 70 dB) is greatest for the L+C, with an area of about 8 city blocks, see Figure 19.

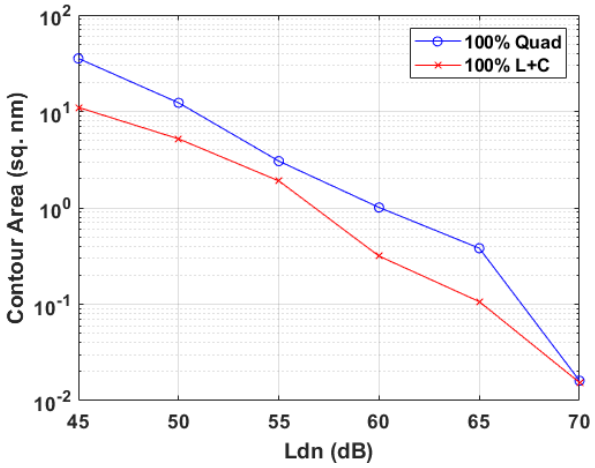

Figure 16: Ldn contour areas over full operations area (arrivals only).

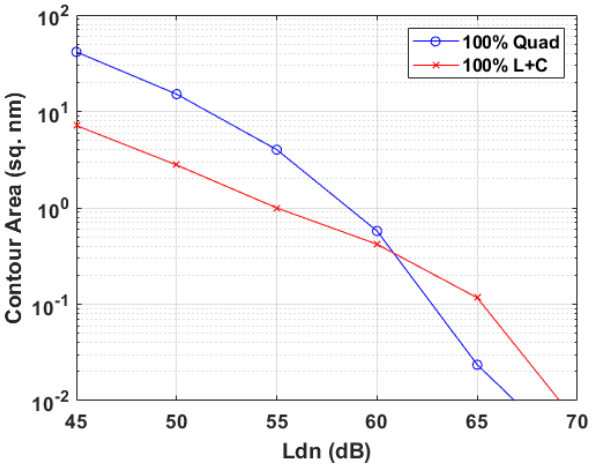

Figure 17: Ldn contour areas over full operations area (departures only).

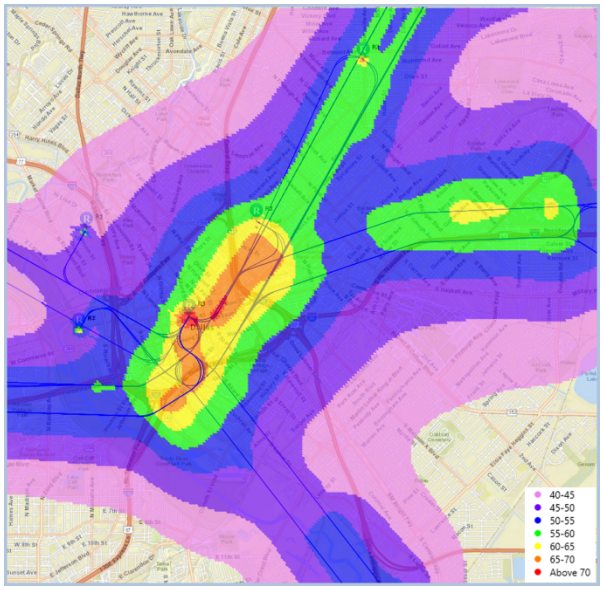

Figure 18: Noise exposure levels, Ldn (dB), near vertiport DF1 for 100% quadrotor (arrival and departure operations).

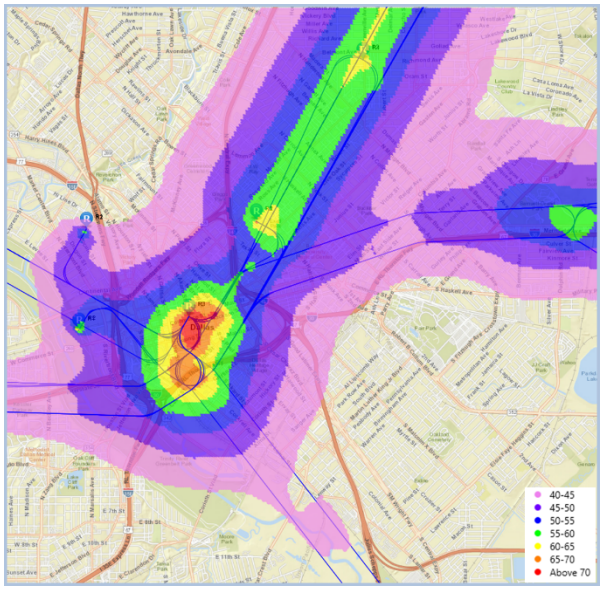

Figure 19: Noise exposure levels, Ldn (dB), near vertiport DF1 for 100% L+C (arrival and departure operations).

A similar trend is noted in the contour areas for arrival operations between the full and vertiport-focused receptor grids (compare Figure 16 with Figure 22). Figure 23 shows that the larger 70 dB contour area for the L+C vehicle in Figure 21 is attributable to departure operations. It also shows that larger contour areas for the L+C relative to the quadrotor occur at a level that is about 5 dB less than seen in full study area (Figure 17).

Finally, it has been observed that airport contour areas around large commercial airports change by a factor of approximately 5.9 for a change in Ldn of 10 dB.[18] In this study, vertiport contour areas in the range of 55-65 dB change, on average, by factors of 6.2, 6.5, and 7.1, for fleets comprised of 100% quadrotor vehicles, 100% L+C vehicles, and a 50/50 quadrotor/L+C vehicle mix, respectively, for a change in Ldn of 10 dB. The UAM and transport aircraft scaling factors are similar because those factors are largely dictated by sound propagation (absorption and spherical spreading loss) and, for takeoff and landing operations, those mechanisms are the same

irrespective of the aircraft type. The remaining differences are attributable to the amount of absorption and spreading loss, which are affected by differences in spectral characteristics and takeoff and landing trajectories between aircraft classes, respectively. Contour areas for en route noise do not scale in the same manner as those near airports because the contours are shaped differently; for straight and level cruise, the contours are generally rectangular (see the en route contours in Figure 12), whereas contours for ascent from and descent to the landing area are more elliptical in shape. Accordingly, when examining the full grid data with a greater amount of en route noise, the same contour areas scale, on average, by factors of 14.4, 9.3, and 14.9, for the 3 mixes respectively, for a change in Ldn of 10 dB.

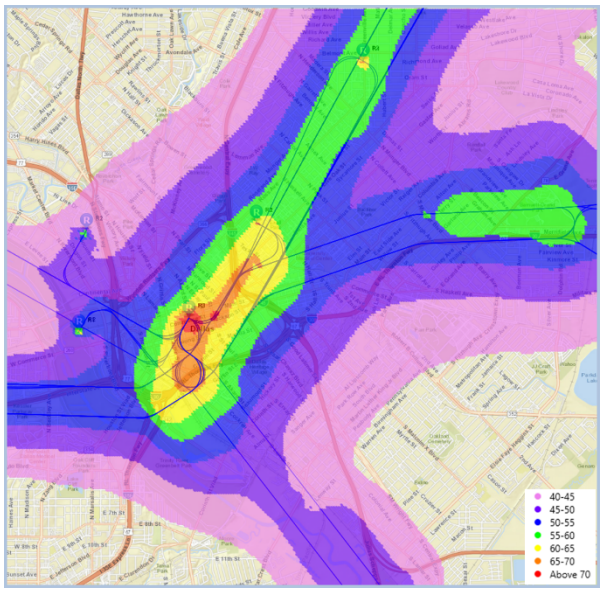

Figure 20: Noise exposure levels, Ldn (dB), near vertiport DF1 for the 50/50 vehicle mix (arrival and departure operations).

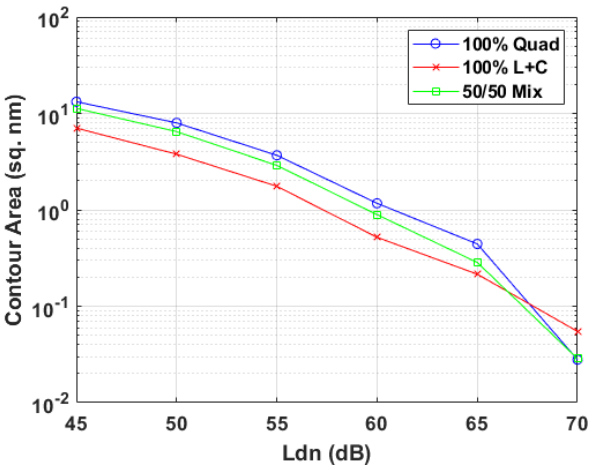

Figure 21: Ldn contour areas corresponding to Figure 18 – Figure 20.

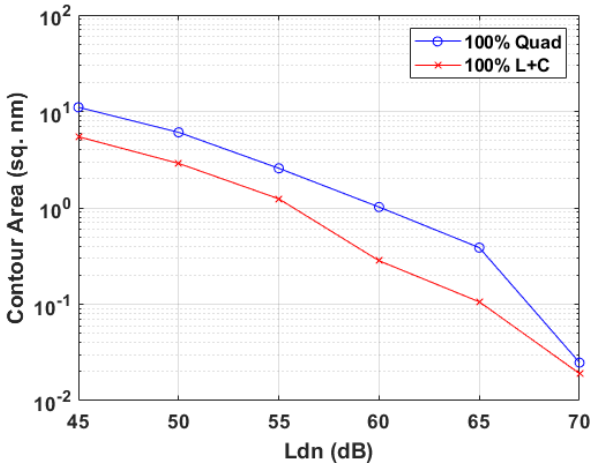

Figure 22: Ldn contour areas near vertiport DF1 (arrivals only).

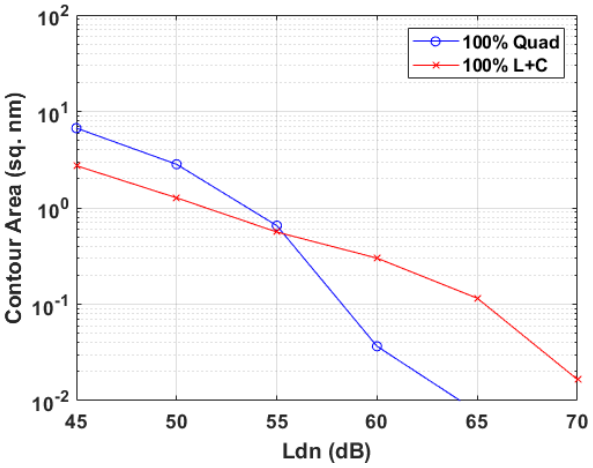

Figure 23: Ldn contour areas near vertiport DF1 (departures only).

VI. Concluding Remarks

A second-generation assessment of community noise due to UAM vehicle operations was conducted using NPD data representing broadband self noise in addition to the periodic loading and thickness noise included in the first-generation assessment. The more extensive route structure and higher volume of operations considered in this work

allowed a more in-depth assessment of noise exposure in the vicinity of vertiports. Differences in noise exposure for different fleet mixes (100% quadrotor, 100% lift+cruise, and a 50/50 mix) were traceable to differences in source noise. It should be noted that the assessments contained herein are of an exemplary nature and may not be generalizable to different route structures or to different vehicles. They are therefore not indicative of what the noise exposure will be for any particular future scenario.

Planned developments to the methodology include use of structured query language (SQL) to facilitate AEDT data input for large studies, and calculation of UAM vehicle NPD data consistent with the helicopter modeling approach in AEDT. This will enable the construction of AEDT studies using the helicopter aircraft type to explore the advantages and disadvantages relative to the fixed-wing aircraft type incorporated in the present methodology. To that end, comparisons with time-marching simulations will provide additional guidance on best modeling practices (fixed-wing, rotary-wing, or hybrid) for different UAM operating scenarios.

Acknowledgments

This work was supported by the NASA Aeronautics Research Mission Directorate, Revolutionary Vertical Lift Technology Project. The authors wish to acknowledge Nelson Guerreiro (NASA Langley) for development of the trajectory data, and Doug Boyd and Stefan Letica (NASA Langley), and Rui Cheng (formerly National Institute of Aerospace) for generation of the Gen 2 NPD data.

References

[1]"Aviation Environmental Design Tool (AEDT) technical manual, Version 3d," U.S. Department of Transportation, Volpe National Transportation Systems Center DOT-VNTSC-FAA-21-06, Cambridge, MA, 2021.

[2]Maurice, L.Q., Lee, D.S., Wuebbles, D.W., Isaksen, I., Finegold, L., Vallet, M., Pilling, M., and Spengler, J., *Final report of the International Civil Aviation Organization (ICAO) Committee on Aviation and Environmental Protection (CAEP) Workshop*, Assessing current scientific knowledge, uncertainties and gaps in quantifying climate change, noise and air quality aviation impacts, L.Q. Maurice, et al., Editors. 2009, US Federal Aviation Administration and Manchester Metropolitan University, Washington, D.C. and Manchester, UK.

[3]Rizzi, S.A., et al., "Urban air mobility noise: Current practice, gaps, and recommendations," NASA TP-2020-5007433, 2020.

[4]Rizzi, S.A. and Rafaelof, M., "Community noise assessment of urban air mobility vehicle operations using the FAA Aviation Environmental Design Tool," *InterNoise 2021*, Virtual Meeting, 2021.

[5]Patterson, M.D., Antcliff, K.R., and Kohlman, L.W., "A proposed approach to studying urban air mobility missions including an initial exploration of mission requirements," *AHS International 74th Annual Forum and Technology Display*, Phoenix, AZ, 2018.

[6]Silva, C., Johnson, W.R., Solis, E., Patterson, M.D., and Antcliff, K.R., "VTOL urban air mobility concept vehicles for technology development," *AIAA AVIATION Forum*, AIAA-2018-3847, Atlanta, GA, 2018, https://doi.org/10.2514/6.2018-3847.

[7]Rimjha, M., Li, M., Hinze, N., Tarafdar, S., Hotle, S., Swingle, H., and Trani, A., "Demand forecast model development and scenarios generation for urban air mobility concepts," Virginia Tech Air Transportation Systems Laboratory Blacksburg, VA, 2020.

[8]Verma, S., Wood, R.D., Dulchinos, V.L., Mogford, R.H., Keeler, J., and Martin, L., "Design and analysis of corridors for UAM operations," To appear as NASA TM, 2022.

[9]Guerreiro, N.M., Butler, R.W., Maddalon, J.M., and Hagen, G.E., "Mission planner algorithm for urban air mobility – Initial performance characterization," *AIAA AVIATION Forum*, AIAA-2019-3626, Dallas, TX, 2019, https://doi.org/10.2514/6.2019-3626.

[10]"Aircraft noise and performance (ANP) database v2.2," EUROCONTROL Experimental Center (EEC), http://www.aircraftnoisemodel.org/, 2018.

[11]Johnson, W.R., "Rotorcraft aerodynamic models for a comprehensive analysis," *AHS International 54th Annual Forum*, Washington, DC, 1998.

[12]Lopes, L.V. and Burley, C.L., "ANOPP2 user's manual: Version 1.2," NASA TM-2016-219342, 2016.

[13]Farassat, F. and Succi, G., "The prediction of helicopter rotor discrete frequency noise," *Vertica*, Vol. 7, 1983, pp. 309-320.

[14]Brooks, T.F., Pope, D.S., and Marcolini, M.A., "Airfoil self-noise and prediction," NASA RP-1218, 1989.

[15]Johnson, W.R., "NDARC — NASA design and analysis of rotorcraft: validation and demonstration," *American Helicopter Society Specialists' Conference on Aeromechanics*, San Francisco, CA, 2020.
[16]van der Wall, B.G., "2nd Higher Harmonic Control (HHC) Aeroacoustic Rotor Test (HART II) - Part I: Test documentation," German Aerospace Center (DLR) IB 111-2003/31, 2003.
[17]"Aviation Environmental Design Tool (AEDT) supplemental manual, AEDT standard input file (ASIF)," U.S. Department of Transportation, Volpe National Transportation Systems Center Supplement to DOT-VNTSC-FAA-21-06, Cambridge, MA, 2021.
[18]Shepherd, K.P., Marcolini, M.A., and Thompson, T.R., "Improved aircraft acoustic technology and its effect on airport community noise impact," NASA TM–2018-219840, 2018.